atmosphere

MDPI

Article

Is Upper-Level Dynamic Forcing Essential for Heavy Rain in the Levant?

Baruch Ziv [1,*] and Uri Dayan [2]

[1] Department of Natural Sciences, The Open University of Israel, Raanana 4353708, Israel
[2] Department of Geography, The Hebrew University of Jerusalem, Jerusalem 9070227, Israel; msudayan@mscc.huji.ac.il
* Correspondence: zivbaruchana@gmail.com

Abstract

This study assesses the effects of upper-level configuration on heavy rain episodes over the Levant. The dynamic upper-level forcings are attributed to ageostrophic effects. One is related to meandering jet ahead of troughs and the second to acceleration near both ends of straight jets. We collected 23 rainy episodes contained in four rainy months. The rain analysis was done on the eastern coast of the Mediterranean, and the synoptic analysis covers the domain 15–45° N, 12–45° E. The data were retrieved from ERA5 reanalysis, with 0.25° × 0.25° resolution. A subjective analysis revealed that the rain episodes are associated with three configurations, the two aforementioned and an additional, under upper trough, without upper-level divergence. In fourteen cases, the region was found ahead of trough and in only one at the end of a straight jet. In the remaining eight cases, upper trough was located over the region, implying an absence of upper-level support for rain formation. These configurations are exemplified by case studies and by composite maps. Most rain events occurred when an upper trough dominated the Levant, situated upstream (west) of a surface Cyprus Low (CL), with both contributing to rain formation. The CL persisted in the cases of the third type, in spite of an absence of upper-level support, due to surface-induced cyclogenesis. The two most frequent configurations are apparently similar but differ in the rain-producing factors. The one for the "ahead of" is upper-level dynamic, and for the "under trough"—lower level dynamic and enhanced static instability.

Keywords: upper-level configuration; heavy rain; Levant; Cyprus Low; jet streak

1. Introduction

The annual rainfall over much of the Levant exceeds 500 mm. This total is comparable to that of major Western European cities such as Paris and Berlin (~650 mm). However, in the Levant, this amount is typically accumulated within 50–80 rain days per year, approximately one-third of the number of rain days in Western Europe. The relatively small number of rain days in the Levant implies a higher frequency of intense rainfall events. For example, the annual average number of days with rainfall exceeding 25 and 30 mm in Tel Aviv, Israel, is 6.2 and 4.5, respectively (based on the Israeli Meteorological Service for the years 1975–2024). On the intra-diurnal scale, rain is often concentrated within a few hours, with a typical amount of 10 mm, e.g., [1,2]. Such intense short-lived rainfall frequently disrupts urban activities and transportation systems. The present study investigates the synoptic-scale factors responsible for events.

Academic Editor: Nirajan Dhakal

Received: 25 March 2026
Revised: 20 May 2026
Accepted: 27 May 2026
Published: 2 June 2026

A major synoptic-scale source of intense rain is upper-tropospheric mass divergence. This has been attributed to several dynamic processes. Newton and Trevison [3] described the upper-level divergence zones that are formed by ageostrophic along-stream winds, related to the curvature variation associated with meandering between troughs and ridges. Another effect is associated with along-stream speed variation, which induces divergence patterns left of the exit and right of the entrance parts of jets [4]. Figure 1a shows, schematically, the divergence centers associated with a meandering jet at the jet axis, ahead of troughs, where the wind turns from super-geostrophic to sub-geostrophic, as it changes curvature from positive to negative. Figure 1b shows the divergence centers associated with the transverse ageostrophic wind component, in response to the violation of the geostrophic balance at the exit and entrance regions of a jet streak. These are found to the left of the exit and to the right of the entrance.

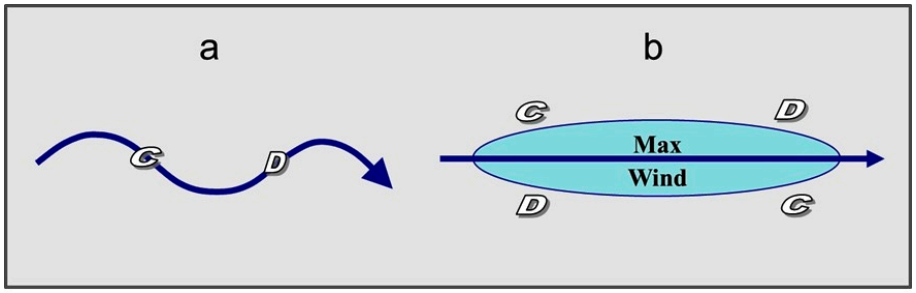

Figure 1. Scheme of the divergence centers associated with (**a**) meandering jet and (**b**) straight jet. Each thick arrow denotes a jet axis. *C* and *D* denote convergence and divergence, respectively, following [4–7].

The upper levels over the Mediterranean region are rather complicated, influenced by both PJ and STJ, e.g., [8]. Dayan and Abramski [9] investigated a major and fatal flooding event in the Middle East that was associated with "very dense clouds along the Jet-stream path" several thousand km long, extending from the ITCZ toward the Caspian Sea, i.e., a tropical plume. Prezerakos [10] showed that synoptic flow patterns leading to the generation of Northwest African depressions were caused by cross-stream ageostrophic components in the entrance and exit regions of jet streaks. Ziv [11] showed that a rainstorm, associated with a tropical plume over the Levant, developed at the inflection region of the STJ ahead of a pronounced mid-latitude trough.

The upper-level conditions that led to a severe flood associated with a Red Sea Trough in south Israel were analyzed by Dayan et al. [12]. They showed that the region was under the divergence center to the left of the exit of a subtropical jet (STJ, hereafter), co-existing with a divergence center to the right of the entrance of a polar jet (PJ, hereafter). An extreme case of cyclogenesis over North Africa was analyzed by Prezerakos et al. [13], who found that a surface cyclogenetic rejuvenation of a migrating Atlas Mountains depression occurred when the "Polar Front-Jet" was positioned to the south of its normal seasonal position and interacted with the STJ, which shifted north of its normal seasonal position. They showed that the divergence center left of the PJ exit overlapped with that of the STJ entrance, which explains the rejuvenation of the surface depression.

Several studies have indicated the existence of significant rains over the Levant while located under an upper-level cyclonic system or even to its west, where divergence is not expected. Kahana et al. [14], in an analysis of 52 major floods in south Israel during the years 1965–94, found that 17 were associated with the 'Syrian Low', i.e., a surface cyclone centered northeast of Israel. A composite map for these floods shows that they took place beneath the axis of the 500 hPa trough, so that no upper-level dynamic was found to be supportive of the flood-producing rain. Rubin et al. [15] showed that, at the final stage of

a rainstorm associated with tropical plume, a surface cyclone was situated at the eastern coast of the Mediterranean, co-locating with a 300 hPa pronounced trough (see Figure 4b in [15]). This produced "scattered rains common to mid-latitude cyclones". In a study of a fatal flood that took place on 26 April 2018, Dayan et al. [16] showed that the area where the main flood occurred was under the influence of a surface low, combined with a cutoff low at the 300 hPa level over the same region (see Figure 4 in [16]). The above examples indicate that significant rains might occur in the Levant without upper-level dynamic forcing inducing ascendance at the mid-levels.

A feature common to the above cases is the presence of a Cyprus Low (CL). This stresses the central role of this surface system as a rain generator for the Levant, including the Syrian Low, a variant of the CL [3]. The CL contributes the vast majority of the total rainfall in north and central Israel (83% according to Saaroni et al. [17]). The rain producing mechanisms associated with the CLs are both thermodynamic and dynamic, as described by Shay-El and Alpert [18]. Cold air masses, originating from Europe become moist and unstable when moving over the warmer water of the EM surface. These air masses, while encountering the shoreline and later on the mountain ridges, are forced to rise and to produce convective rains. The resulting rain, observed over ~50 km onshore, is more intense than over the sea [19].

The present study is a necessary attempt to bridge the gap between the individual case studies described above and an automatic analysis for the upper-level patterns, with which heavy rainfall is associated, such as that done by Wu et al. [20]. Our approach follows ZAMG [21], who analyzed 100 convective systems over the Iberian Peninsula and France during the period 1992–2009, with seven of them in the form of trains, with lengths of hundreds of kilometers, all ahead of a cold front. As major conditions for train generation, they mentioned an LLJ near 925 hPa and the convergence of specific humidity at 1000 hPa.

Our aim is to identify the leading upper-level configurations dominating intense winter rainfall over the Levant. A special focus is given to heavy rains that occur beneath an upper-level trough axis where no dynamical forcing is present. Section 2 specifies the methodology and materials. Section 3 presents case studies and composite maps for the various configurations, and Section 4 discusses and summarizes the results.

2. Materials and Methods

The analysis is based on the configuration of the upper-level flow with which heavy rains in the Levant are associated. The area of interest covers the eastern Mediterranean coast, extending for approximately 100 km of the shoreline on both sides. The data were collected from 4 rainy winter months: January 1969, December 1991, February 2003 and January 2018, in which more than 250 mm (~2 times the monthly average) fell over the northern half of Israel. The following is based on the 23 episodes, in which at least 5 mm within 3 h and 20 mm of daily rainfall were observed over the study region. Since the rainfall is taken from a gridded database, and the actual rain is mainly convective, the actual rainfall, in particular for 3 h interval, is expected to be considerably higher.

The cases analyzed are those in which one configuration was identified as dominant. The first is associated with meandering flow ahead of a trough, the second, with along-stream acceleration at the end of a jet, and the third, with cyclonic flow under a trough. For convenience, they are entitled, hereafter, as 'ahead of trough', 'at jet end' and 'under trough' types, respectively. Table 1 specifies the dates and times of the cases according to the three configurations.

Table 1. Cases according to the dominant configuration. For the 'at jet end', only one case (5 January 1969 00 UTC) was found, and is therefore not included.

Ahead of Trough														
	1	2	3	4	5	6	7	8	9	10	11	12	13	14
Date	21 January 1969	22 January 1969	28 January 1969	3 December 1991	8 December 1991	11 December 1991	31 December 1991	3 February 2003	19 February 2003	24 February 2003	5 January 2018	14 January 2018	18 January 2018	25 January 2018
Hour (UTC)	09	12	18	06	18	18	00	15	21	03	03	00	18	09
Under Trough														
	1	2	3	4	5	6	7	8						
Date	22 January 1969	24 January 1969	12 December 1991	24 February 2003	25 February 2003	5 January 2018	14 January 2018	19 January 2018						
Hour (UTC)	18	00	00	21	12	12	12	03						

The synoptic analysis is based on data taken from ERA5 [22], over the eastern part of the Mediterranean, i.e., 20–45° N, 15–45° E, with 0.25° × 0.25° resolution. The basic variables used were the 2 horizontal wind components at 300 hPa level. This level lies between that of the STJ, found near 200 hPa, and the PJ (around 350 hPa), both found to be involved in the rain events (see Section 3 below). This agrees with Yang et al. [23]. They were used to depict the wind field for identifying the upper-level configuration. The relative vorticity field was extracted via GrADS (Grid Analysis and Display System) software (Doty 1995. http://opengrads.org/, accessed on 31 May 2026) [24]. In addition, we used the sea level pressure (SLP), rainfall ("total precipitation" tp) and the Total Totals index (*TT*, [25]) to assess the static instability, all from the ERA5 reanalysis database. The *TT* is defined as

$$TT = (T_{850} - T_{500}) + (Td_{850} - T_{500}), \quad (1)$$

where T and Td are the temperature and dew point, respectively, and the subscript denotes the pertinent pressure level. This index indicates the extent to which the lower levels are warmer than the middle levels and how much warmer they are. The *TT* index was preferred over the *K* index (*KI*, [26]), also offered by the ERA5 database, *KI*, and defined as

$$KI = (T_{850} - T_{500}) + Td_{850} - (T_{700} - td_{700}). \quad (2)$$

The *TT* was chosen, because the *KI* gives double weight to the absolute temperature in the lower levels, which makes it less suitable for the winter rains analyzed here.

The choice of ERA5 rainfall data is based on their advantage in capturing the coastal amplifying effect characterizing the eastern coast of the Mediterranean [27]. In order to identify occurrences of the desired configuration, we manually scanned the relevant maps, in 3 h intervals, in an attempt to find an optimal match between intense rain and a distinct upper-level configuration.

3. Results

The 23 cases are first presented in Section 3.1 and then analyzed through composite maps in Section 3.2.

3.1. Case Studies

This part presents the three configurations.

3.1.1. 'Ahead of Trough'

The 'ahead of trough' configuration was identified in 14 cases, exemplified here by 18 January 2018 18 UTC. The wind field (Figure 2a) shows a pronounced trough, extending from the Black Sea through southwest Turkey, toward the Nile Delta (along 32° E longitude). Two parallel jets are denoted, and the PJ dominates the EM.

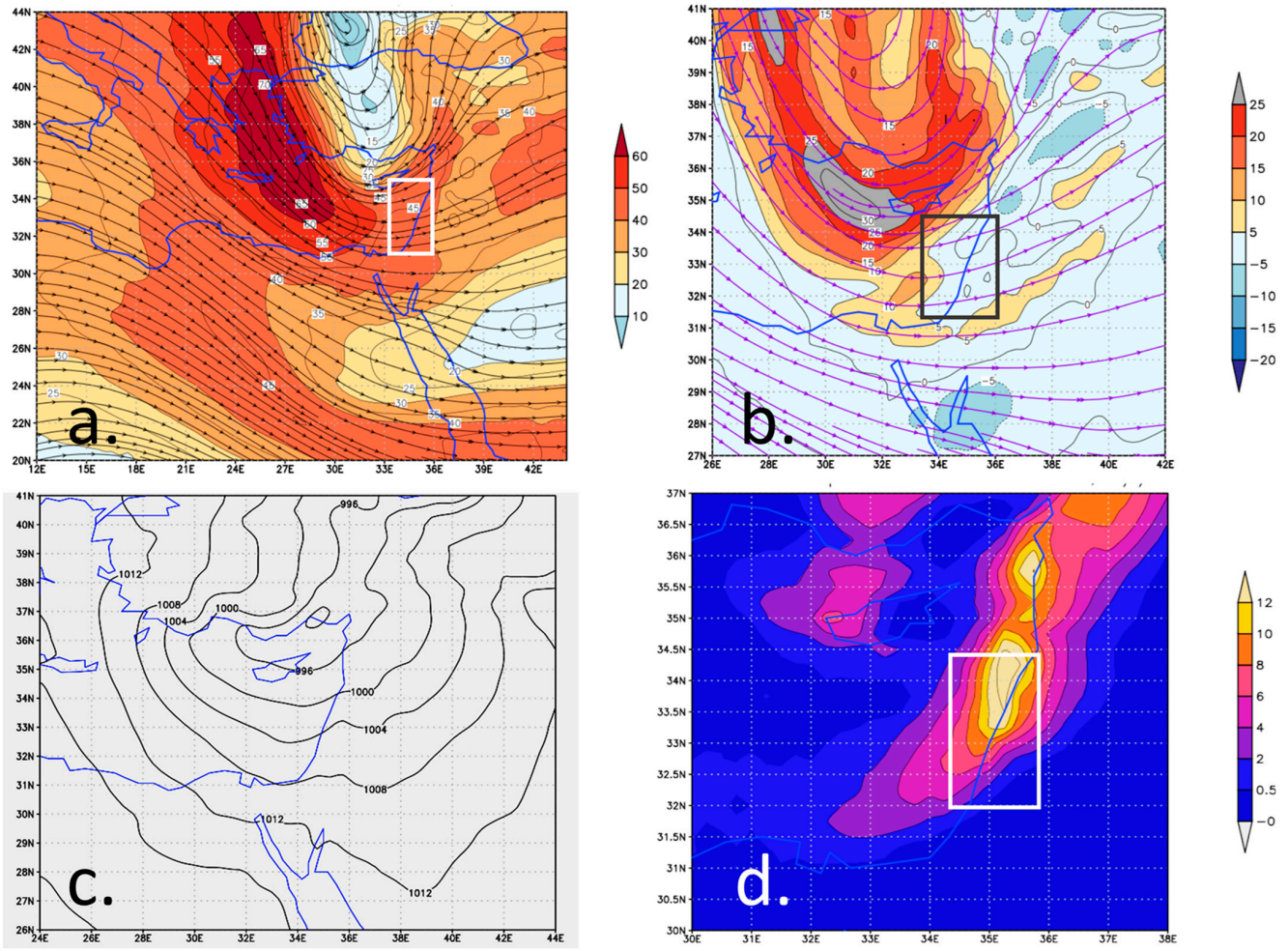

Figure 2. The case of 18 January 2018 18 UTC. (**a**) Wind field at 300 hPa, with streamlines (black) and wind speed (ms^{-1}, colored shading). (**b**) Relative vorticity at 300 hPa ($s^{-1} \times 10^5$, colored shading). (**c**) Sea level pressure (SLP), with 4 hPa intervals. (**d**) Rainfall (mm) during the 3 h centered over 18 UTC. The rectangles in (**a**,**b**,**d**) denote the study area.

The Levant was positioned under the inflection region of the PJ, ahead of the trough. The vorticity map (Figure 2b) shows high values, ~30×10^{-5} s^{-1}, west of the Levant, in tandem with the westerly wind. This implies intense positive vorticity advection over the Levant. The rain map (Figure 2d) indicates a prominent rainband extending along the eastern coast of the Mediterranean, from Turkey southward, with rates exceeding 14 mm within 3 h, a rather high rate in synoptic terms. The intense rain can be attributed to the

ageostrophic effect imparted by a change in the curvature of the flow ahead of the trough, as well as to the effect of the well-developed CL, with a minimum pressure of 992 hPa (Figure 2c).

3.1.2. 'At Jet End'

The 'at jet end' configuration was barely identifiable, found to be dominant only in one case within the study period. In another two cases, associated with along-stream acceleration, the jet streaks were considerably curved, so that the rain was attributable mainly to one of the 'ahead of trough' configurations. The case identified is shown below in Figure 3.

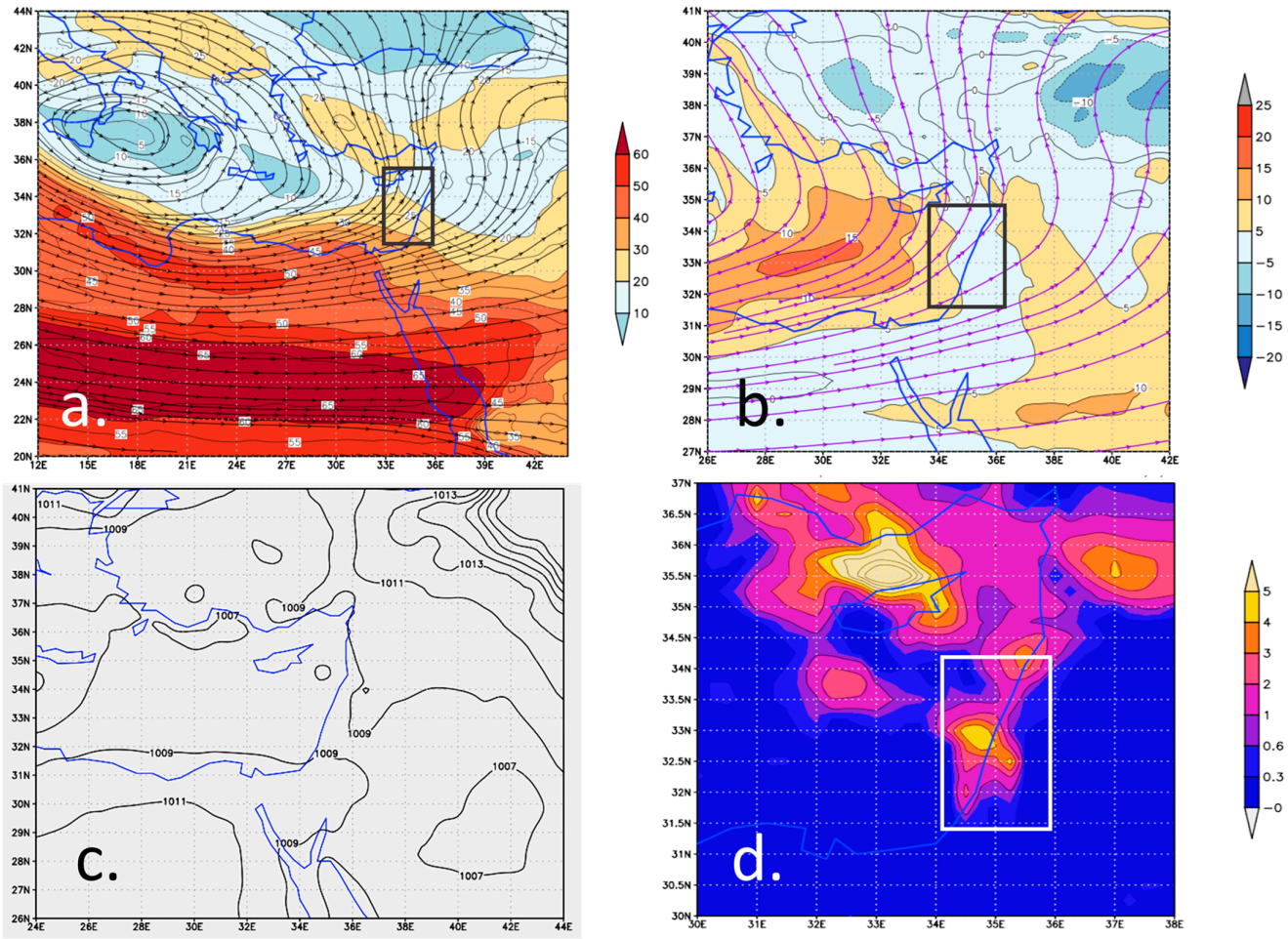

Figure 3. The case of 5 January 1969 00 UTC. (**a**) Wind field at 300 hPa, with streamlines (black) and wind speed (ms^{-1}, colored shading). (**b**) Relative vorticity at 300 hPa ($s^{-1} \times 10^5$, colored shading). (**c**) Sea level pressure (SLP), with 2 hPa intervals. (**d**) Rainfall (mm) during the 3 h centered over 18 UTC. The rectangles in (**a**,**b**,**d**) denote the study area.

In the upper-levels, a closed cyclone dominated the central Mediterranean, elongated in a west–east orientation. Two jets are identified: a PJ, extending eastward along the North African coasts, around 30° N latitude, and an STJ, over North Africa, around 24° N latitude. Both are more or less zonal and almost straight (Figure 3a). The exit of the PJ was found over the Levant; so, the study region was at the left side of the sector with along-stream deceleration, implying divergence. We suggest that despite the jet's slight curvature, the acceleration effect dominated. This is supported by the vorticity field (Figure 3b), which shows negligible values east of Cyprus, despite the pronounced curvature of the streamlines in that area. Conversely, the vorticity is positive southwest of Cyprus, reaching

approximately 15×10^{-5} s^{-1}, where the streamlines are nearly straight. This emphasizes the dominance of shear vorticity over curvature, characterizing jet entrances and exits. In this case, the maximum rain rate was less than 5 mm in 3 h and covered only a limited portion of the Levant (Figure 3d). This can be attributed to a weak signature of the CL, in this case, 1008 hPa, with a weak gradient (Figure 3c), the weakest of all 23 cases.

3.1.3. Cyclonic Curvature

The cyclonic curvature type is exemplified by the 5 January 2018 12 UTC event, in which an upper-level trough covered the EM and the Levant (Figure 4a). No consistent vorticity advection was noted at this time (Figure 4b). The lower levels were dominated by a pronounced CL (1002 hPa), centered between Cyprus and Lebanon (Figure 4c). Since no dynamic forcing was identified in the upper-level, the CL seems to be the main cause for the intense rain that was observed over the Levant, with centers of over 10 mm within 3 h (Figure 4d).

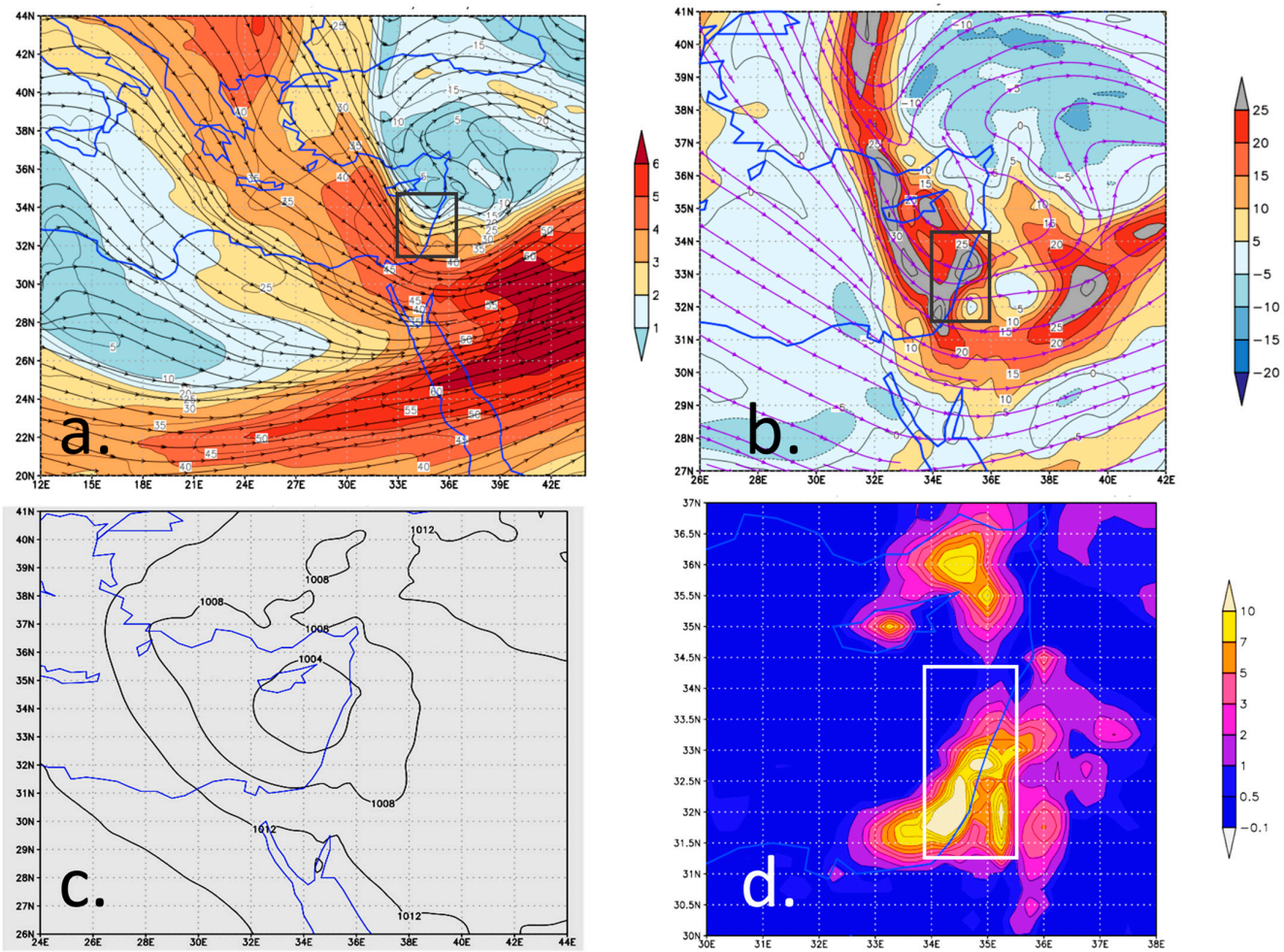

Figure 4. The case of 5 January 2018 12 UTC. (**a**) Wind field at 300 hPa, with streamlines (black) and wind speed (ms^{-1}, colored shading). (**b**) Relative vorticity at 300 hPa ($s^{-1} \times 10^5$, colored shading). (**c**) Sea level pressure (SLP), with 2 hPa intervals. (**d**) Rainfall (mm) during the 3 h centered over 18 UTC. The rectangles in (**a**,**b**,**d**) denote the study area.

3.2. Composite Analysis

Compositing enables information from a number of examples of a phenomenon to be combined in a convenient format that highlights the basic common features of the various types, while eliminating the detail of individual cases [28]. The calculated composite mean

is commonly used to resolve relationships between large-scale atmospheric circulations and meteorological or hydrological phenomena. Kahana et al. [14] applied composite analysis to identify the typical synoptic factors inducing major flashfloods over southern Israel. Composite analysis was applied in this study only for the two leading configurations, because the 'at jet end' type was identified as dominant only once. This includes upper atmospheric vorticity and wind charts, SLP charts and rain maps (Figure 5). We also produced composite maps of the upper-level temperature anomaly and the *TT* index (Figure 6).

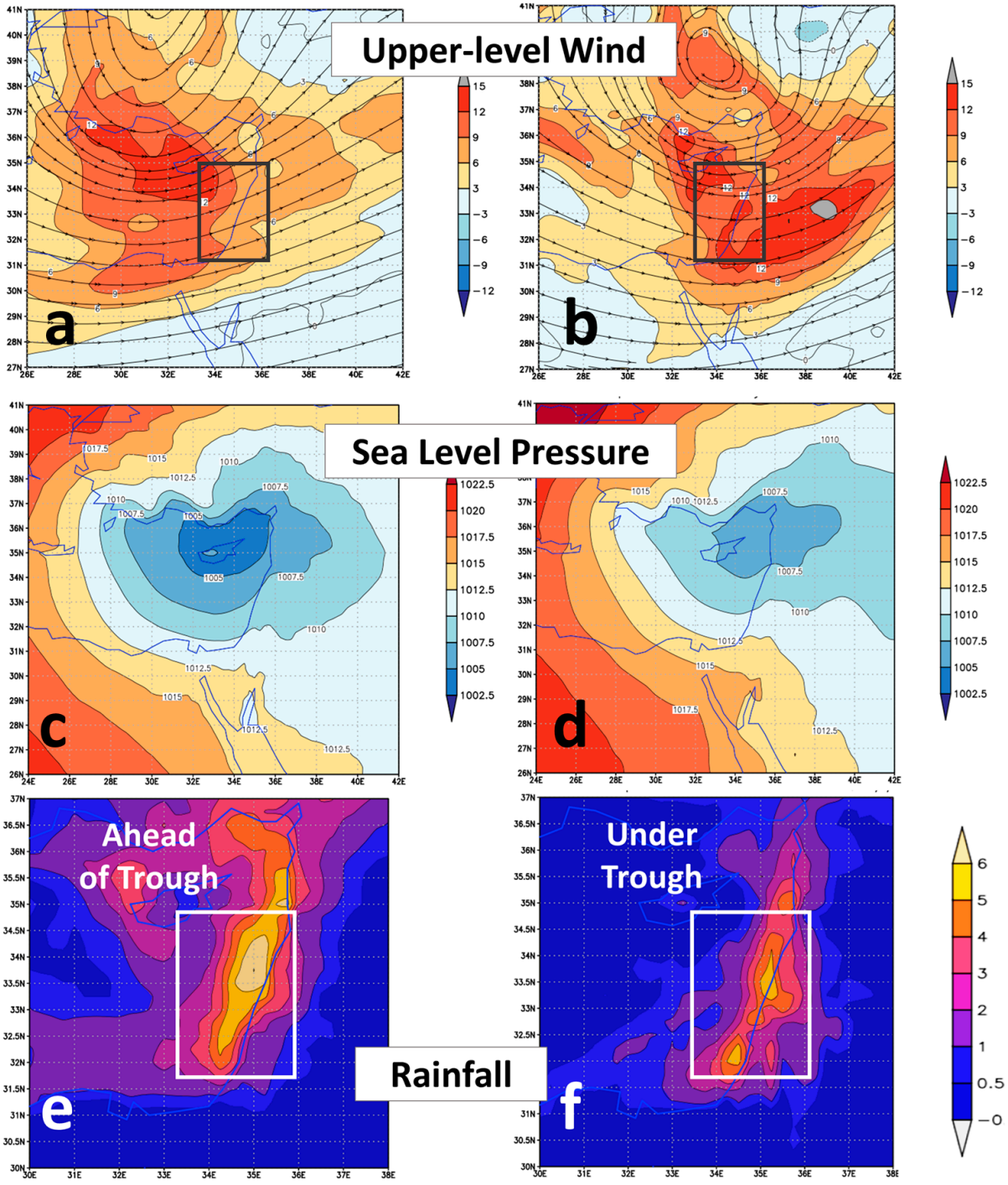

Figure 5. Composite maps for the cases associated with 'ahead of trough' type (14 cases, (**a**,**c**,**e**) and 'under trough' type (8 cases, (**b**,**d**,**f**), including relative vorticity at 300 hPa ($s^{-1} \times 10^5$, colored shading). SLP (hPa, (**c**,**d**), with 2 hPa intervals) and 3 h rainfall (mm, (**e**,**f**)). The rectangles in (**a**,**b**,**e**,**f**) denote the study area.

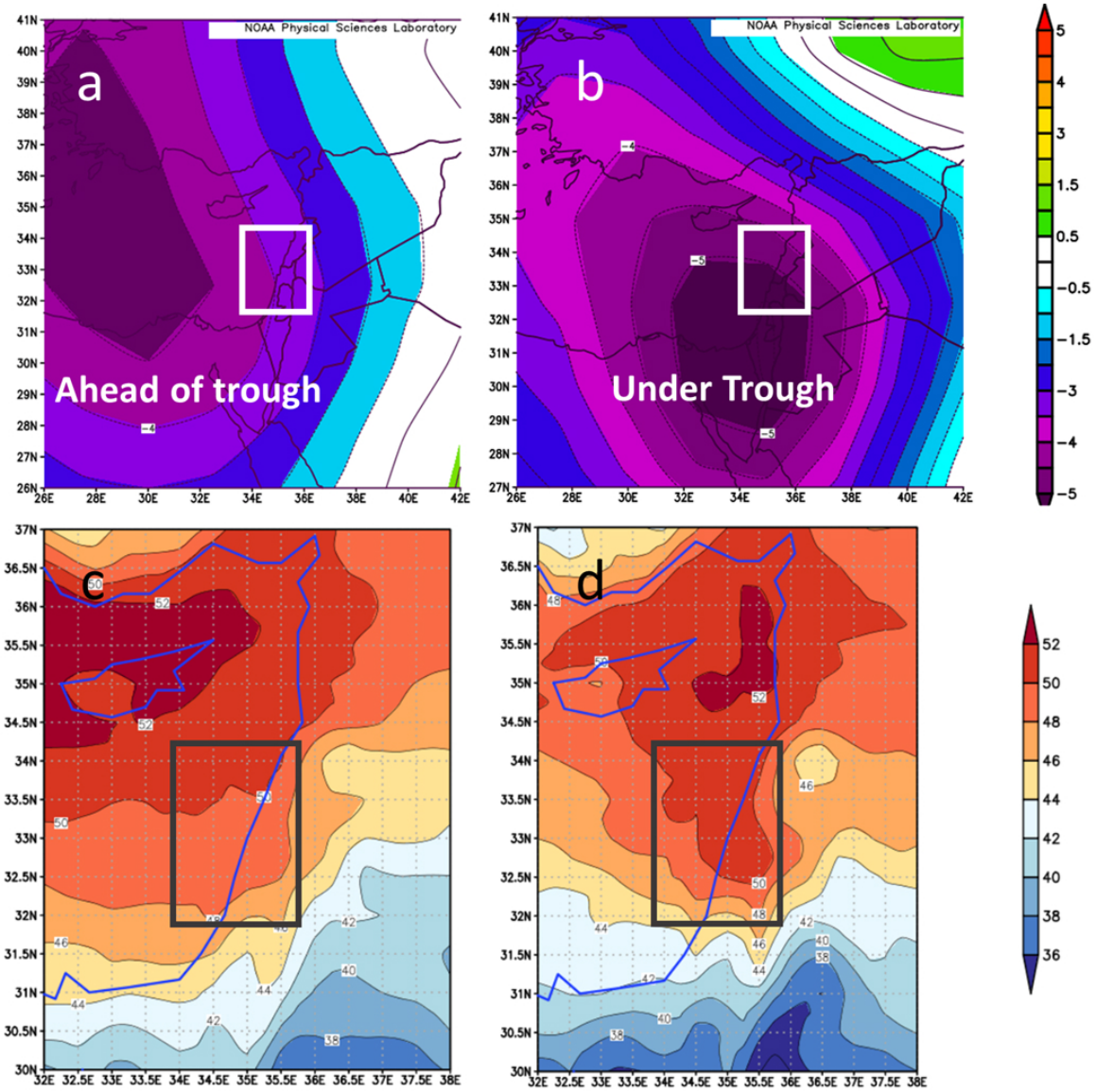

Figure 6. Composite temperature anomaly at 700 hPa level for the 'ahead of trough' and 'under trough' ((**a**) and (**b**), respectively) and the Total Totals index for the two types (**c**) and (**d**), respectively). The temperature anomaly is based on the NCEP-NCAR reanalysis data [29] The rectangles in all of the panels denote the study area.

The two 300 hPa vorticity composite maps (Figure 5a,b) show a dominant trough over the EM, with the vorticity exceeding 12×10^{-5} s^{-1}. The SLP maps (Figure 5c,d) exhibit distinct CLs centered at 36° N for both types. The rain distribution (Figure 5e,f) for both types shows considerable rain rates over the Levant, reaching 5 mm in 3 h, slightly lower than these found for the individual cases. This artifact stems from the inherent smoothing resulting from the spatial spread of the individual rain maxima. The maximum intensity for both types is centered along the EM coast, in a range of 50–100 Km offshore. This distribution is consistent with the observational analysis of CLs, based on TRIMM satellites, found by Heiblum et al. [19].

The vorticity field of the 'ahead of trough' differs from that of the 'under trough' by the location of the upper-level trough (and the vorticity maximum). The location for the former is along 30.5° E, as compared to 34.5° E for the latter, corresponding to the coastline. This implies positive vorticity advection over the Levant for the 'ahead of trough' and not for the 'under trough' configuration. Another difference between these two types is in the

wind configuration over southeastern Europe and the EM. The flow with which the 'ahead of trough' type is associated is mostly an open trough extending from Europe toward the EM, while for the 'under trough' type a cut-off low dominates (compare Figure 5a,b).

The CL corresponding to the 'ahead of trough' (Figure 5c) type is found 2° west of that corresponding to the 'under trough' type (at 34° E) and is deeper by ~3 hPa (Figure 5d). The longitudinal displacement between the upper-level trough and the surface cyclone is ~3° for the 'ahead of trough' type and only ~1.5° for the 'under trough' type. The rainfall maps show a major advantage of the 'ahead of trough' type, expressed both in rain intensity and extension, mainly to the west.

The fact that, in the Levant region, heavy rainfall occurred in eight events without upper-level forcing prompted us to examine the significant thermodynamic factor in CLs, namely instability. To this end, we investigated the thermal conditions during these events. The factor examined was the intrusion of polar air associated with the upper-level troughs. This was addressed by composites of mid-level temperature anomalies, represented by the 700 hPa and the temperature difference between 1000 and 600 hPa. The anomaly maps for the 'ahead of trough' and 'under trough' (Figures 6a and 6b, respectively) show a negative center of 5 K, demonstrating a pronounced polar intrusion: for the 'ahead of trough' at the Nile Delta and for the 'under trough' over the Levant itself. The impact of this shift in the anomaly between the two types is reflected by a larger vertical temperature difference over the Levant for the latter type, indicating further instability there, as reflected by the average value of the Total Totals index over the majority of the Levant, by over 1. Compare Figure 6c,d.

4. Summary and Discussion

The present study documents the dominating upper-level configurations during heavy rain events over the Levant. The analysis was conducted on four rainy months. Fifteen events were identified as associated with one of the two basic configuration types of diverging flow: fourteen at the inflection region ahead of an upper-level trough and only one to the left side of the exit of a straight jet streak. A separate group, which had been noted in the literature, was found here in eight cases, associated with the core of an upper-level trough. In each of the 23 cases analyzed, a Cyprus Low (CI) dominated the lower levels. It should be noted that, while all the upper-level configurations coexist with heavy rain events, the third configuration is the one that is not its direct cause.

Contrary to near-surface cyclonic flow, which favors rain formation, upper-level cyclonic flow by itself does not contribute to rain production. In the cases associated with the 'under trough' configuration, the lack of upper-level dynamic support is further emphasized by the absence of vorticity advection, as implied by Figure 5b. Hence, the rain can be attributed to near-surface convergence resulting from the Cyprus Low (CL), which dominates the Levant in these cases (as reflected in Figure 5d) and its related effects, as explained in Section 1).

We identified fourteen cases as 'ahead of trough' and only one case 'at jet end'. The scarcity of cases associated with a straight jet may be explained by the curved flow induced by the upper-level troughs dominating rain events over the Levant [30]. The cases belonging to 'ahead of trough' are characterized by open troughs west of the Levant, whereas the 'under trough' type is dominated by a cutoff low over Turkey, with a pronounced trough over the Levant itself (compare Figures 5a and 5b, respectively). The differences in intensity and location explain the southeasterly shift of the −5 K isotherm of the 700 hPa temperature anomaly toward the Levant for the 'under trough' type (Figure 6a,b). The 700 hPa temperature anomaly over the Levant is negative in both, but its value over the southeastern Mediterranean is 1.5–2 K lower for the 'under trough' type. The presence of

the colder air above the warm sea surface implies further instability in the air approaching the EM coastline and, subsequently, intensifies the convective rains. This effect is estimated by a comparison of the composite maps of the Total Totals (*TT*) index for the two configuration types. The *TT* for the 'under trough' was higher by 1 degree over that of the 'ahead of trough'. We suggest that a similar index, in which the 500 hPa is replaced by 700 hPa (unfortunately, not common) would yield even a larger difference. Such an index can serve for rain prediction rather than for thunderstorms, as the *TT* and the *KI* do.

The presence of CLs and upper-level in each of the 23 cases analyzed stresses the linkage between the upper-level troughs and the CLs and between the CLs and the rain itself. The cyclogenesis is evident whenever the CL is found east of the upper trough, as in the 'ahead of trough' cases, as manifested by the composite maps (Figure 5). In the 'under trough' cases, the CL is almost co-located with the upper trough. They are separated by 1.5° on average, and in four cases, they are co-located. This reflects the mature stage of mid-latitude cyclones, when the upper-level induced cyclogenesis weakens or even ceases. The fact that five out of the eight 'under trough' cases followed cases of 'ahead of trough' within 12 h implies that the 'under trough' configuration is an optional continuation of the 'ahead of trough' one. This raises the question of what maintains the CL at that stage. It can be attributed to EM regional cyclogenetic features, such as the Taurus Mountains in south Turkey and sensible and latent heat flux from the Mediterranean warmer sea surface [31,32].

During the four months analyzed, there was no case in which the divergence centers of two jets coincided or reinforced each other, as found by Dayan et al. [12]. It should be noted that the 'at jet end' type was the less frequent, though it had been reported as being associated with-rain producing systems other than CLs, over the Levant, i.e., the Red Sea Trough [12,14] and tropical plumes [9,15]. This does not mean that Red Sea troughs are absent during the winter but suggests that their contribution to intense rains during the winter months is marginal.

The contribution of the present study is the establishment of three configurations in the upper-level flow with which winter heavy rains in the Levant are associated. Another outcome is the finding that the CL is the dominant rain producing mechanism, even when the upper-level forcing ceases to support it. The upper-level configurations found here can contribute to upgrade the widely used automatic Alpert et al. [33] synoptic classification for the Levant, which is based on the lower levels alone.

The weakness of the present study is its limited climatological basis due to the small study period. Another flaw stems from our subjective approach in the identification of the various cases. An objective automatic approach, used by Wu et al. [20] for predicting extreme rain in China through, based on one straight jet, could not be applied at this stage. This is due to the complexity of the dual jet (STJ and PJ) interactions and their meandering character over the Levant. It should be noted that our trials to obtain quantitative thresholds for identifying the upper-level patterns were not fruitful. For instance, we calculated the vorticity advection field from the wind data, but this field was found noisy even after smoothing. We hope that a machine learning approach will be able to classify the configurations, based on the patterns identified manually in this study.

This study examined the relative roles of upper-level dynamics and low-level processes in winter heavy-rain events over the Levant. It addresses the question of whether upper-level dynamic forcing is essential for heavy rain in the Levant. The results indicate that such forcing is not always essential for the direct development of heavy rain. Nevertheless, upper-level dynamics remain an important indirect contributor, both through their role in the formation and development of the CL, which provides the primary synoptic

environment for rainfall, and through their enhancement of atmospheric instability, which can intensify precipitation.

Author Contributions: B.Z.: Conceptualization, Visualization, Methodology, Writing; U.D.: Initiation, Data curation, Writing. All authors have read and agreed to the published version of the manuscript.

Funding: The authors thank the Israeli Science Foundation (ISF, grant number 2899/24).

Institutional Review Board Statement: Not applicable.

Informed Consent Statement: Not applicable.

Data Availability Statement: The data used in this study are publicly available at the Copernicus Climate Change Service (C3S), 2017: ERA5: Fifth generation of ECMWF atmospheric reanalyses of the global climate. Copernicus Climate Change Service Climate Data Store (CDS). https://cds.climate.copernicus.eu./datasets (accessed on 1 May 2025).

Conflicts of Interest: The authors declare no conflicts of interest.

References

1. Goldreich, Y. *The Climate of Israel: Observation, Research and Application*; Springer: Berlin/Heidelberg, Germany, 2003.
2. Ziv, B.; Dayan, U.; Shendrik, L.; Vadislavski, E. 2024: Intense rains in Israel associated with the train effect. *Nat. Hazards Earth Syst. Sci.* **2024**, *24*, 3267–3277. [CrossRef]
3. Newton, C.W.; Trevison, A. Cyclogenesis and frontogenesis in jet stream waves, Part I: Analytic relations to wave structure. *J. Atmos. Sci.* **1984**, *41*, 2717–2734. [CrossRef]
4. Keyser, D.; Shapiro, M.A. A review of the structure and dynamics of upper-level frontal zones. *Mon. Wea. Rev.* **1986**, *114*, 452–499. [CrossRef]
5. Uccellini, L.W.; Kocin, P.J. The interaction of jet—streak circulations during heavy snow events along the east coast of United States. *Wea. Forecast.* **1987**, *2*, 289–308. [CrossRef]
6. Kocin, P.J.; Uccellini, L.W.; Petersen, R.A. Rapid evolution of a jet streak circulation in a pre-convective environment. *Meteor. Atmos. Phys.* **1986**, *35*, 103–138. [CrossRef]
7. Shaffie, S.; Mozaffari, G.; Khosravi, Y. Climatic analysis of effective jet streams frequency on extreme precipitations in west of Iran. *J. Water Clim. Change* **2021**, *12*, 787–800. [CrossRef]
8. Harnik, N.; Galanti, E.; Martius, O.; Adam, O. The Anomalous Merging of the African and North Atlantic Jet Streams during the Northern Hemisphere Winter of 2010. *J. Clim.* **2014**, *27*, 7319–7334. [CrossRef]
9. Dayan, U.; Abramski, R. Heavy Rain in the Middle East Related to Unusual Jet Stream Properties. *Bull. Am. Meteorol. Soc.* **1983**, *64*, 1138–1140. [CrossRef]
10. Prezerakos, N.G. Synoptic flow patterns leading to the generation of Northwest African depressions. *Int. J. Climatol.* **1990**, *10*, 33–48. [CrossRef]
11. Ziv, B. A subtropical rainstorm associated with a tropical plume over Africa and the Middle-East. *Theor. Appl. Climatol.* **2001**, *69*, 91–102. [CrossRef]
12. Dayan, U.; Ziv, B.; Margalit, A.; Morin, E.; Sharon, D. A severe autumn storm over the middle-east: Synoptic and meso-scale convection analysis. *Theor. Appl. Clim.* **2001**, *69*, 103–122. [CrossRef]
13. Prezerakos, N.G.; Flokas, H.A.; Brikas, D. The role of the interaction between polar and subtropical jet in a case of depression rejuvenation over the Eastern Mediterranean. *Meteorol. Atmos. Phys.* **2006**, *92*, 139–151. [CrossRef]
14. Kahana, R.; Ziv, B.; Enzel, Y.; Dayan, U. Synoptic climatology of major floods in the Negev Desert, Israel. *Int. J. Clim.* **2002**, *22*, 867–882. [CrossRef]
15. Rubin, S.; Ziv, B.; Paldor, N. Tropical Plumes over Eastern North Africa as a Source of Rain in the Middle-East. *Mon. Weather Rev.* **2007**, *135*, 4135–4148. [CrossRef]
16. Dayan, U.; Lensky, I.M.; Ziv, B.; Khain, P. Atmospheric conditions leading to an exceptional fatal flash flood in the Negev Desert, Israel. *Nat. Hazards Earth Syst. Sci.* **2021**, *21*, 1583–1597. [CrossRef]
17. Saaroni, H.; Halfon, N.; Ziv, B.; Alpert, P.; Kutiel, H. Links between the rainfall regime in Israel and location and intensity of Cyprus lows. *Int. J. Clim.* **2010**, *30*, 1014–1025. [CrossRef]
18. Shay-El, Y.; Alpert, P. A diagnostic study of winter diabatic heating in the Mediterranean in relation to cyclones. *Q. J. R. Meteorol. Soc.* **1991**, *117*, 715–747. [CrossRef]
19. Heiblum, R.H.; Koren, I.; Altaratz, O. Analyzing coastal precipitation using TRMM observations. *Atmos. Chem. Phys.* **2011**, *11*, 13201–13217. [CrossRef]

20. Wu, R.; Zhu, P.; He, P.; Zhang, W.J. Configurations of the East Asian jet stream for extreme precipitation in central eastern China during June. *Clim. Dyn.* **2025**, *63*, 203. [CrossRef]
21. ZAMG: Cumulonimbus (Cb) and Mesoscale Convective System, (MCS): Special Investigation: The Train Effect or Train Mechanism. Available online: https://resources.eumetrain.org/satmanu/CMs/Cb/navmenu.php?page=7.0.0 (accessed on 24 March 2026).
22. Hersbach, H.; Bell, B.; Berrisford, P.; Biavati, G.; Horányi, A.; Muñoz Sabater, J.; Nicolas, J.; Peubey, C.; Radu, R.; Rozum, I.; et al. ERA5 hourly data on pressure levels from 1940 to present. *Copernic. Clim. Change Serv. Climate Data Store* **2023**. [CrossRef]
23. Yang, Y.; Carey-Smith, T.; Turner, R. The merged and superposed sub-tropical jet and polar-front jet in the southwest Pacific: A case study. *Atmos. Sci. Lett.* **2024**, *25*, e1203. [CrossRef]
24. Doty, B. *The Grid Analysis and Displa System (GrADS) Version 1.5 User's Guide*; Center for Ocean-Land-Atmosphere Studies (COLA): Fairfax, VA, USA, 1995; 398p.
25. Miller, R.C. Notes on Analysis and Severe-Storm Forecasting Procedures of the Air Force Global Weather Central. In *AWS Technical Report 200 (Revised)*; Air Weather Service, U.S. Air Force: Bellevue, NE, USA, 1972.
26. George, J.J. Weather Forecasting for Aeronautics. In *An Introduction to Dynamic Meteorology*, 3rd ed.; Holton, J.R., Ed.; Academic Press: San Diego, CA, USA, 1960; 511p.
27. Tatli, H. Nonlinear precipitation patterns in the Mediterranean and Middle East: Insights from ERA5 reanalysis (1940–2024). *Environ. Earth Sci.* **2025**, *84*, 406. [CrossRef]
28. Sinclair, M.R.; Revell, M.J. Classification and composite diagnosis of extratropical cyclogenesis events in the southwest Pacific. *Mon. Weather Rev.* **2000**, *128*, 1089–1105. [CrossRef]
29. Kalnay, E.; Kanamitsu, M.; Kistler, R.; Collins, W.; Deaven, D.; Gandin, L.; Iredell, M.; Saha, S.; White, G.; Woollen, J.; et al. The NCEP=NCAR 40-Year Reanalysis Project. *Bull. Am. Meteorol. Soc.* **1996**, *77*, 437–471. [CrossRef]
30. Zangvil, A.; Druian, P. Upper-air trough axis orientation and the spatial distribution of rainfall distribution over Israel. *Int. J. Clim.* **1990**, *10*, 57–62. [CrossRef]
31. Stein, U.; Alpert, P. Factor separation in numerical simulations. *J. Atmos. Sci.* **1993**, *50*, 2107–2115. [CrossRef]
32. Flaounas, E.; Gray, S.L.; Teubler, F. A process-based anatomy of Mediterranean cyclones: From baroclinic lows to tropical-like systems. *Weather Clim. Dynam.* **2021**, *2*, 255–279. [CrossRef]
33. Alpert, P.; Osetinsky, I.; Ziv, B.; Shafir, H. Semi-objective classification for daily synoptic systems, application to the Eastern Mediterranean climate change. *Int. J. Climatol.* **2004**, *24*, 1001–1011. [CrossRef]